

Mechanical High-Intensity Focused Ultrasound (Histotripsy) in Dogs With Spontaneously Occurring Soft Tissue Sarcomas

Lauren Ruger , Ester Yang, Jessica Gannon, Hannah Sheppard , Sheryl Coutermarsh-Ott, Timothy J. Ziemlewicz, Nikolaos Dervisis, Irving C. Allen , Gregory B. Daniel , Joanne Tuohy , Eli Vlasisavljevich , and Shawna Klahn

Abstract—Introduction: Histotripsy is a non-invasive focused ultrasound therapy that uses controlled acoustic cavitation to mechanically disintegrate tissue. To date, there are no reports investigating histotripsy for the treatment of soft tissue sarcoma (STS). **Objective:** This study aimed to investigate the *in vivo* feasibility of ablating STS with histotripsy and to characterize the impact of partial histotripsy ablation on the acute immunologic response in canine patients with spontaneous STS. **Methods:** A custom 500 kHz histotripsy system was used to treat ten dogs with naturally occurring STS. Four to six days after histotripsy, tumors were surgically resected. Safety was determined by monitoring vital signs during treatment and post-treatment physical examinations, routine lab work, and owners' reports. Ablation was characterized using radiologic and

histopathologic analyses. Systemic immunological impact was evaluated by measuring changes in cytokine concentrations, and tumor microenvironment changes were evaluated by characterizing changes in infiltration with tumor-associated macrophages (TAMs) and tumor-infiltrating lymphocytes (TILs) using multiplex immunohistochemistry and differential gene expression. **Results:** Results showed histotripsy ablation was achievable and well-tolerated in all ten dogs. Immunological results showed histotripsy induced pro-inflammatory changes in the tumor microenvironment. **Conclusion & Significance:** Overall, this study demonstrates histotripsy's potential as a precise, non-invasive treatment for STS.

Index Terms—Ablation, cancer, canine, focused ultrasound, histotripsy, immuno-oncology, soft tissue sarcoma.

Manuscript received 15 June 2022; revised 28 July 2022; accepted 21 August 2022. Date of publication 25 August 2022; date of current version 20 February 2023. The work of Lauren Ruger was supported by the Virginia Tech ICTAS Doctoral Scholars Program. The work of Shawna Klahn was supported by the NIH National Center for Advancing Translational Sciences through iTHRIV Scholars Program under Grants UL1TR003015 and KL2TR003016. This work was supported by the Focused Ultrasound Foundation under Grant 453047. (Lauren Ruger and Ester Yang contributed equally to this work.) (Corresponding authors: Eli Vlasisavljevich; Shawna Klahn.)

Lauren Ruger, Jessica Gannon, and Hannah Sheppard are with the Department of Biomedical Engineering and Mechanics, Virginia Polytechnic Institute and State University, USA.

Ester Yang, Nikolaos Dervisis, Gregory B. Daniel, and Joanne Tuohy are with the Department of Small Animal Clinical Sciences, Virginia-Maryland College of Veterinary Medicine, USA, and also with the Virginia Tech Animal Cancer Care and Research Center, Virginia-Maryland College of Veterinary Medicine, USA.

Sheryl Coutermarsh-Ott and Irving C. Allen are with the Department of Biological Sciences and Pathobiology, Virginia Polytechnic Institute and State University, USA.

Timothy J. Ziemlewicz is with the Department of Radiology, University of Wisconsin-Madison, USA.

Eli Vlasisavljevich is with the Department of Biomedical Engineering and Mechanics, Virginia Polytechnic Institute and State University, Blacksburg, VA 24061 USA (e-mail: eliv@vt.edu).

Shawna Klahn is with the Department of Small Animal Clinical Sciences, Virginia-Maryland College of Veterinary Medicine, Blacksburg, VA 24061 USA, and also with the Virginia Tech Animal Cancer Care and Research Center, Virginia-Maryland College of Veterinary Medicine, Roanoke, VA 24061 USA (e-mail: klahn@vt.edu).

This work involved animals in its research. Approval of all ethical and experimental procedures and protocols was granted by the Virginia Tech Institutional Animal Care and Use Committee (#20-049).

This article has supplementary downloadable material available at <https://doi.org/10.1109/TBME.2022.3201709>, provided by the authors.

Digital Object Identifier 10.1109/TBME.2022.3201709

I. INTRODUCTION

HIGH intensity focused ultrasound (HIFU) is a non-invasive ablation technique with the ability to destroy tissue by thermal or mechanical means. While traditional HIFU relies on the absorption of ultrasound energy to thermally destroy tissue, histotripsy is a non-thermal technique that uses repeated short pulses of ultrasound waves to mechanically disintegrate tissue into a liquefied acellular debris [1], [2], [3], [4]. Histotripsy applies short (1–10 cycles), high pressure (>15–30 MPa) pulses to produce inertial cavitation, which form a precise histotripsy bubble cloud at the targeted location within the tissue [5], [6]. The subsequent rapid expansion and collapse of these bubbles causes mechanical disruption of the cellular structure, reducing treated tissues to emulsified acellular debris that can be absorbed as part of the body's physiologic healing process [3], [7]. Histotripsy treatment is typically guided in real-time by ultrasound imaging, allowing the precise, non-invasive targeting of tissues ranging from deep, visceral structures to superficial, subcutaneous tumors. Previous preclinical studies have shown that histotripsy can successfully ablate various tumor types *ex vivo* and *in vivo* [4], including prostate [8], kidney [9], bone [10], brain [11], pancreatic [12], and liver tumors [13], [14]. Additionally, a recent human clinical trial has shown safe and effective ablation of primary and metastatic liver tumors [15]. The results of these prior studies suggest that histotripsy has the potential to be a paradigm-shifting method for image-guided,

non-invasive tumor ablation. While widely explored for other tumor types, histotripsy not yet been explored for the ablation of superficial soft tissue sarcoma tumors.

In addition to its ablative potential, histotripsy may also promote immunostimulatory effects related to its ability to induce immunogenic cell death [16]. Studies of HIFU in rodent tumor models have demonstrated that HIFU is immunogenic and that histotripsy may result in more robust immune responses than thermal HIFU [17], [18], [19]. The *in situ* tumor debris remaining after mechanical ablation may include tumor neoantigens in their native form, preserving immunogenicity and the potential to generate a systemic immune response against tumor cells. These tumor neoantigens can be recognized by antigen presenting cells, activating immune effector cells and initiating immune cell infiltration. The resulting antitumor immune response may then stimulate local and systemic immune responses [19]. Early studies investigating these effects have reported that histotripsy treatment in a murine cancer model can alter the tumor microenvironment and activate an immune response [9], [12], [15], [16], [18], [19], [20]. Similarly, a case of an abscopal effect was identified in the human clinical trial investigating histotripsy for liver tumor ablation [21]. These findings, combined with prior work showing that thermal HIFU can target and treat soft tissue sarcoma (STS) tumors in both dogs [22], [23], [24] and humans [25], [26], [27], have led our team to initiate this study to investigate histotripsy's ablative and immunological effects for treating STS in pet dogs.

Soft tissue sarcomas (STS) are a common cancer in dogs and arise from mesenchymal tissues, representing different types of tumors with similar histologic features and biologic behavior. STS comprise of 15% of all skin and subcutaneous tumors in dogs, but are rare tumors in humans, comprising only 1% of all adult malignancies [28], [29]. In both species, STS are rapidly growing tumors with low metastatic potential, but locally aggressive behavior. The complexity of the tumor is characterized by its variable presentation and behavior, and treatment typically requires a multimodal approach. Adequate local tumor control requires either complete removal of the tumor with extensive surgical resection of adjacent grossly normal tissue or a combination of surgery and radiation therapy to address microscopic disease, reducing the risk of recurrence. As a result, novel techniques are still needed to treat soft tissue sarcoma while preserving adjacent healthy tissue.

Spontaneous tumors in pet dogs are also increasingly recognized for their value in translational oncology research [30], [31]. Naturally-arising cancers in dogs provide a cancer research model to address pre-clinical questions and challenges through their genetic diversity, tumor heterogeneity, and by following similar biological and therapeutic courses as their human counterparts. Canine cancers arise naturally within the complex interactions between the tumor, the tumor microenvironment, and the host immune system, providing a unique opportunity to evaluate and refine immunotherapy strategies [32], [33], [34]. Therefore, in addition to its direct implications for veterinary medicine, the investigation of histotripsy's ablative and immunological effects on canine STS in this study provides an opportunity to

advance medical knowledge and therapies for a human disease for which the low tumor incidence can make recruitment of sufficient human patients challenging.

The objective of this study was to demonstrate the *in vivo* safety and feasibility of ablating soft tissue sarcomas with histotripsy in canine patients with spontaneous STS. Our secondary objective was to characterize the impact of the histotripsy ablation on the acute immunologic response in the tumor microenvironment. A custom 500 kHz histotripsy system was used to treat ten client-owned dogs with soft tissue sarcomas in order to test whether histotripsy could achieve safe and effective ablation of targeted tumor regions in dogs with naturally occurring STS tumors. Four to six days after histotripsy treatment, tumors were surgically resected. Radiologic (i.e., CT) and histopathology assessments were conducted to determine (1) the efficacy of the histotripsy ablation and (2) the impact of a single histotripsy treatment within a portion of the STS on the immunologic response.

II. MATERIALS AND METHODS

A. Study Design

1) Study Population, Screening, and Enrollment Criteria:

This was a prospective, single-arm, open-label pilot study of histotripsy treatment in dogs with soft tissue sarcomas. Client-owned dogs with naturally-occurring tumors presented to the Animal Cancer Care and Research Center (ACCRC) over an 8-month period (September 2, 2020 - May 10, 2021) were recruited for enrollment. The owners of eligible dogs were offered standard treatment options, including palliative care. Informed consent was obtained for all enrolled dogs. This study was approved by the University Institutional Animal Care and Use Committee (#20-049) and the College of Veterinary Medicine Hospital Board.

Canine patients with cytologic or histological diagnosis of a peripheral, malignant soft tissue tumor were considered for enrollment. Inclusion and exclusion criteria parameters were selected to ensure that enrolled canine patients would likely result in evaluable data: patients were healthy enough to undergo multiple anesthetic events, the tumor was malignant, treatable with histotripsy, and resectable, and the patient would survive the entire study period. Tumor-specific inclusion criteria were a diameter of at least ≥ 2 cm; an accessible solid area for treatment; and, surgically resectable, as determined by an ACVS-board-certified surgeon who is a surgical oncology fellow. Patients were required to undergo routine laboratory bloodwork, and thoracic and abdominal imaging at screening. The patient had to have an expected survival time of >6 weeks without treatment. Patients were excluded if the tumor was non-resectable or if the recommended surgical resection was declined, if the patient had definitive therapy other than surgery within the past 3 weeks, or if a co-morbidity precluded anesthesia: significant cardiac dysfunction, creatinine value $>1.2x$ the upper reference limit (URL), ALT or AST values $>3.0x$ the URL, or total bilirubin value $>1.2x$ URL.

2) Evaluation Timeline:

Within 10 days prior to treatment, baseline evaluation included an examination; Complete Blood

Count (CBC) and serum biochemistry; tumor measurements using calipers and gross photographs; contrast CT scan (SOMATOM Confidence RT) of the thorax, abdomen, and tumor; and pre-treatment biopsy. The pre-treatment biopsy was performed outside of the planned treatment zone. On the day of histotripsy treatment, a physical exam was completed and tumor photographs were obtained immediately prior to and immediately following treatment. One day post-treatment, an exam, CBC, serum biochemistry, and contrast CT scan of the tumor were performed, and tumor measurements and photographs were collected. Four to six days post-treatment, tumor measurements and photographs, CBC, serum biochemistry, and contrast CT scan of the tumor were performed immediately prior to surgical resection. This timepoint was selected based on prior work with thermal HIFU in dogs with soft tissue sarcomas [24]. Surgical excision and post-operative recommendations for all canine patients were directly performed or supervised by an oncology-fellowship-trained Diplomate of the American College of Veterinary Surgeons (ACVS). Patients were examined and the surgery site was photographed two weeks after surgery. Post-study monitoring recommendations were at clinician discretion, including monthly physical exams and thoracic radiographs appropriate to the patient's tumor type and stage. Patient outcome was documented by communication with the owner or primary-care veterinarian.

B. Safety and Feasibility of Histotripsy Treatment

1) Histotripsy System and Pressure Calibration: In this study, a 32-element, 500 kHz histotripsy transducer with a coaxially aligned 3 MHz curvilinear ultrasonic imaging probe (Model C5-2, Analogic Corp., Peabody, MA, USA) was used. The transducer had a geometric focus of 78 mm with elevational and transverse aperture sizes of 112 mm and 128 mm, respectively, and corresponding f-numbers of 0.70 (elevational) and 0.61 (transverse). The array transducer was built in-house using rapid prototyping technology and integrated onto a prototype clinical histotripsy system (HistoSonics, Ann Arbor, MI, USA) before treatment [Fig. 1]. After aligning the imaging probe coaxially within the therapy transducer, the transducer assembly was attached to a triaxial robotic micro-positioner mounted on the clinical system via an articulating arm. The transducer was driven using a custom high-voltage pulser designed to generate single cycle therapy pulses and controlled by a preprogrammed field-programmable gate array (FPGA) board (Altera DE0-Nano Terasic Technology, Dover, DE, USA). The transducer was powered by a high voltage DC power supply (GENH750W, TDK-Lambda, National City, CA, USA) and controlled by a custom MATLAB script (The MathWorks, Natick, MA, USA) written to receive a trigger from the clinical system.

Before treatment, focal pressure waveforms for the 500 kHz transducer were measured using a high-sensitivity reference rod hydrophone (HNR-0500, Onda Corp., Sunnyvale, CA, USA) and a cross-calibrated custom-built fiber optic hydrophone (FOPH) in degassed water at the transducer's focal point [35], [36]. The rod hydrophone was also used to measure the lateral, elevational, and axial 1-D focal beam profiles of the transducer

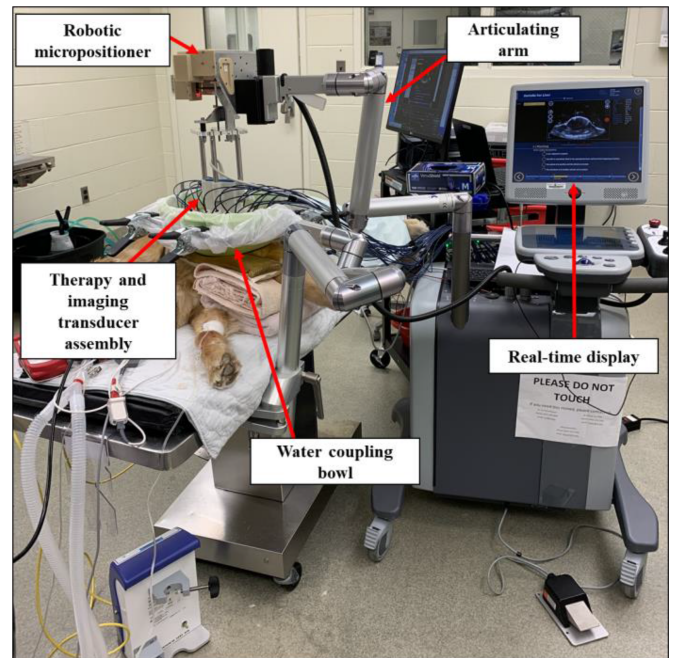


Fig. 1. Experimental histotripsy set-up. A robotic micro-positioner is connected to an articulating arm supporting the therapy and imaging transducer assembly. The transducer assembly was submerged in a water coupling bowl coupled to the patient's tumor, and treatment was monitored in real-time using ultrasound imaging.

by scanning the hydrophone incrementally over a distance wider than the focal width at a peak negative pressure (p_-) of ~ 1.8 MPa. The measured transverse, elevational, and axial full-width half-maximum (FWHM) dimensions at the geometric transducer were measured to be 2.1 mm, 2.1 mm, and 6.6 mm, respectively. Focal pressures were measured directly with the FOPH up to a peak negative pressure of ~ 20 MPa; at peak negative pressures greater than ~ 20 MPa, the focal pressure was estimated by summing measurements from a subset of a quarter and a half of the total elements to prevent cavitation from forming on the fiber. All waveforms were measured using a Tektronix TBS2000 series oscilloscope at a sample rate of 500 MS/s; then, the waveform data was averaged over 128 pulses and recorded in MATLAB.

2) Histotripsy Treatment: Patient-specific treatment plans were developed using pre-treatment CT images, physical examinations, and freehand ultrasound imaging. Patients were anesthetized following standard protocols for client-owned dogs. Anesthesia was maintained using inhaled isoflurane, and anesthesia parameters were measured every five minutes (blood pressure, pulse, and ventilation) or every fifteen minutes (oxygen saturation, carbon dioxide saturation, body temperature, and cardiac arrhythmias). The treatment area was clipped and closely-shaved using a razor to remove overlying fur. The histotripsy transducer was positioned over the treatment site and placed in a container of degassed water ($<30\%$ dissolved O_2) coupled to the canine patient to ensure acoustic propagation from the transducer to the skin. Fine adjustments to correctly position the transducer over the targeted region were made using the robotic micro-positioner.

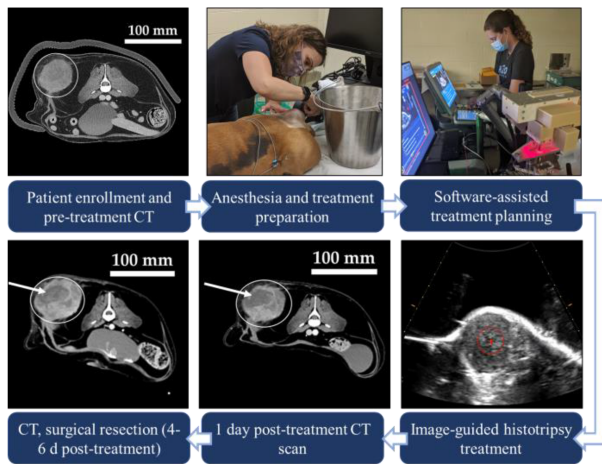


Fig. 2. Study workflow. After patient-specific treatment plan development, fur was removed and patients were anesthetized. An automated histotripsy treatment was conducted using custom planning software. Post-treatment images were collected before surgical resection of the tumor.

Each tumor was treated with histotripsy according to the patient-specific treatment plan using one cycle pulses applied at a pulse repetition frequency (PRF) of 500 Hz. Prior to the volumetric treatment, the pressure at the focus was increased incrementally until a visible bubble cloud was generated on ultrasound imaging. A spherical treatment volume fully contained within the tumor was set manually within the software of the system. After identifying a pressure level for treatment and setting the treatment boundaries, an automated volumetric histotripsy was applied to a 3D grid of equidistant treatment points within the defined boundaries. Treatment points were spaced by 3.5 mm in the axial direction and 1.5 mm in the lateral and elevational directions to allow overlap between the bubble cloud at each location. The robotic micro-positioner moved the focus between treatment locations, and each point was treated with ~ 500 pulses. The transducer frequency and treatment PRF used in this study were chosen to minimize the treatment time required to ablate the large STS tumors [6], [37], and the treatment dosage was chosen based on previous histotripsy studies for other soft tissue applications [12], [14], [38], [39]. The bubble cloud and tissue effects were monitored during treatment using real-time ultrasound imaging. The histotripsy treatment workflow is summarized in Fig. 2.

3) Evaluation of Safety and Scoring of Adverse Events: Safety was monitored with physical examinations, owner-reported outcomes, CBC, and serum biochemistry profiles. Adverse events (AEs) were graded according to the Veterinary Cooperative Oncology Group-Common Terminology Criteria for Adverse Events (VCOG-CTCAE v1.1) [40]. Severe adverse events (SAEs) were defined as any grade 4/5 toxicity.

4) Evaluation of Ablation Effectiveness: Tumor ablation was evaluated for targeting feasibility and ablation completeness through a combination of ultrasound imaging, contrast-enhanced CT images, and gross and microscopic tissue evaluation. Ultrasound imaging was used to confirm the formation of the histotripsy bubble cloud during histotripsy treatment and to monitor for echogenicity changes in the treated

tissues after ablation. Contrast CT scans were performed at three timepoints (baseline, one day post-treatment, and four to six days post-treatment) and analyzed to determine changes in overall tumor volume post-treatment and to measure ablated tissue volumes. All CT measurements were completed by a fellowship-trained radiologist with extensive experience evaluating oncologic imaging who was blinded to planned histotripsy treatment volumes (T.J.Z.). Differences between pre- and post-treatment tumor volumes as well as differences between 1 day post- and 4 day-post treatment ablation zone dimensions were compared using two-tailed and one-tailed paired student's t-tests, respectively. Immediately following surgical removal, the tumor was sectioned and gross photographs were obtained identifying the ablation zone. Representative sections of the pre-treatment tumor, treated tumor, treatment interface, and untreated tumor were fixed in 10% formalin for at least 24 hours and embedded in paraffin. A standard hematoxylin and eosin (H&E) stain was used to stain all tissues to assess the extent of histotripsy damage to the tissue. All sections were evaluated by a veterinary pathologist and Diplomate of the American College of Veterinary Pathologists (ACVP) with extensive experience evaluating ablated tumor tissue (S.C.O.).

C. Evaluation of the Immunological Impact

1) Multiplex Immunohistochemistry (mIHC): Optimized chromogenic multiplex immunohistochemistry (IHC) was performed on formalin-fixed, paraffin-embedded (FFPE) samples in order to investigate the presence and phenotype of infiltrating immune cells following histotripsy treatment. Two multiplex IHC panels were applied to treated and untreated tumor samples from the same patient and then compared. Tumor-associated macrophages (TAMs) and tumor-infiltrating lymphocytes (TILs) were investigated. The Roche Ventana Discovery Ultra Automated Research Stainer (Roche Diagnostics, Indianapolis, IN) was used according to the manufacturer's instructions for IHC multiplexing. To characterize TAMs, tissues were stained with antibodies against pan-macrophage marker IBA-1 (FujiFilm, 019-19741, 1:300), M1-polarization marker iNOS (Abcam, ab3523, 1:100), and M2-polarization marker CD206 (NovusBio, NBP190020, 1:200). To characterize TILs, tissues were stained with antibodies against pan T-cell marker CD3 (DAKO, A0452, 1:100), helper T-cell marker CD4 (Origene, TA500477, 1:100), cytotoxic T-cell marker CD8 (Invitrogen, PAS-16893, 1:100), and regulatory T-cell marker FOXP3 (Invitrogen, 14-7979-82, 1:100). Signals were generated using the following chromagens: IBA-1 and CD4, purple; iNOS and CD8, teal; CD206 and CD3, yellow; and FOXP3, DAB (Roche Diagnostics, Indianapolis, IN). Multiplex-stained slides were evaluated by a veterinary pathologist (S.C.O.).

2) Gene Expression: Tumor microenvironment gene expression was evaluated with the NanoString Canine IO panel (XT-CIO-12, NanoString, Seattle, WA). RNA was extracted using the RNeasy FFPE kit (Research Products International Quick-RNA FFPE MiniPrep, RPI-ZR1008) following manufacturer instructions. Pre-treatment RNA was extracted from formalin-fixed paraffin-embedded (FFPE) soft tissue tumor scrolls of sections of pre-treatment samples, or from untreated

tumor if pre-treatment samples were inadequate. Post-treatment RNA was extracted from FFPE scrolls of sections of the interface between treated and untreated tumor. RNA was normalized to 20ng/uL and hybridized with a target-specific Reporter and Capture Probes (CodeSet) with the nCounter Prep station at 65 °C for 18 hours. Sample data was acquired with the nCounter scanner. Background signal was reduced by subtracting threshold counts of 20 and normalization was performed with housekeeping genes using the nSolver 4.0 software.

3) Serum Cytokine Analysis: Multiplex serum cytokine analysis was performed using a commercially available canine-specific antibody-coated Bead-Based Multiplex Assay to quantify 13 cytokines in each sample (CCYTMG-90K-PX13, Millipore Sigma, Burlington, MA). The following cytokines were measured: GM-CSF, IFN γ - IL-2, IL-6, IL-7, IL-8, IL-15, IP-10 (CXCL10), KC-like (CXCL1), IL-10, IL-18, MCP-1 (CCL2), and TNF- α . The assay was performed according to the manufacturer's directions. Samples were randomized on the plate. The samples were incubated overnight at 4 °C and a magnetic plate washer was utilized. All standards, quality controls, and samples were analyzed in duplicate on Luminex 200 multiplexing instrument (Luminex Corp, Austin, TX). Sample analyte concentrations were generated utilizing standard curve data from each run via Belysa curve fitting software (Millipore Sigma, Burlington, MA).

D. Statistical Analysis

Cytokine analysis results were evaluated for normal distribution with the D'Agostino's K-squared test. For normally distributed data, continuous variables were tested using the repeated-measures t-test, and categorical variables were tested using the Chi Square test. For skewed data, continuous variables were tested using either Wilcoxon test or the Cochran's Q test. Data for serum concentrations of inflammatory cytokines were normalized using log₁₀ transformation and then analyzed using a paired, two-tailed t-test. All p-values were 2-sided, and p-values <0.05 were considered to be statistically significant. All cytokine statistical analyses were performed using GraphPad Prism 9 (GraphPad Software, San Diego, CA). The analytes pre- and/or post-treatment did not read for all patients and were excluded from statistical testing where appropriate.

For Nanostring gene expression results, sample values were log₂ transformed to a variance plot to assess for differentially expressed (DE) genes using heteroscedastic *t* test ($p < 0.05$) per manufacturers' recommendations. DEs were analyzed using agglomerative clustering (Euclidean distance), fold changes and *p* values were reported for each DE on the ROSALINDTM software 3.35.40.

III. RESULTS

A. Patient Population

Ten canine patients with spontaneous STS were enrolled in this study. Five female and five male dogs from different breeds (1 Boxer, 1 Bichon Frise, 1 Border Collie, 1 Great Dane, 1 Miniature Schnauzer, 1 Beagle, and 4 Mixed Breed Dogs) and

aged 7-12 years received histotripsy treatment 4 to 6 days before surgical excision of the tumor. The characteristics of the canine patients, as well as, the grade, subtype, excision status, and location of the treated tumors are summarized in **Table I**.

In all dogs, the tumor was well visualized on the pretreatment CT scan and measured at least 2 cm in diameter. The histologic diagnosis of the tumors included 3 grade III STS, 4 grade II STS, 2 grade I STS, and 1 malignant mesenchymoma. For the tumors in which subtypes were included on the histopathology report, 3 perivascular wall tumors, 2 myxosarcoma, 1 malignant mesenchymoma, and 1 fibrosarcoma were diagnosed. After histotripsy treatment, eight dogs had their tumors completely excised with <0.1 – 0.5 cm margins where noted (margins not reported for all patients). In two dogs (Patients #1 and #2 in **Table I**), complete excision of the tumor was not achievable due to the extensive invasion of the tumor into healthy surrounding tissues and anatomic restrictions limiting the surgical window.

Patient outcome was followed for a median of 112 days (range: 14-285 days). Six dogs are still alive, three dogs were euthanized, and one dog was lost to follow up. All instances of euthanasia were determined to be unrelated to the histotripsy treatment. Two dogs were euthanized due to progressive disease typical of STS: one had recurrence of the grade II STS, and the other had evidence of lung metastasis suspected secondary to the grade III STS. The third dog was euthanized due to development of a retrobulbar mass and immune-mediated thrombocytopenia unrelated to the STS diagnosis.

B. Safety and Feasibility of Histotripsy Treatment

1) Adverse Event Assessment: No significant AEs impacting patient outcome were noted in any of the patients. Anesthesia complications unrelated to histotripsy were reported in three patients, resolving naturally or with standard intervention during treatment. Another patient experienced a vagal response from pain that may be secondary to histotripsy treatment, although the exact cause remains unknown. The remaining six patients had no anesthetic abnormalities. During treatment, body temperatures were maintained between 97.1 °F–102.5 °F for nine patients with one patient experiencing moderate hypothermia at 96.4 °F that resolved with external heat. Pulse rates were maintained between 45–130 bpm for nine patients, with one patient experiencing cardiac dysrhythmia and an asystole cardiac rhythm. The suspected cause of this dysrhythmia is a vagal response from pain, as mentioned above, and the arrhythmia resolved on its own without any medical intervention. Mean blood pressures were maintained between 60–165 mmHg, with one patient experiencing persistent hypotension at 40 mmHg that resolved with fluid therapy. Oxygen saturation levels were maintained between 91–100%. End tidal carbon dioxide levels were maintained at 26–52 mmHg, with one patient experiencing persistent respiratory depression at 59 mmHg secondary to spontaneous breathing and resolved after increasing isoflurane gas. No complications were reported during anesthetic recovery in any of the patients.

No clinically significant AEs associated with histotripsy treatment were reported through bloodwork, post-treatment physical

TABLE I
PATIENT DEMOGRAPHICS AND TUMOR CHARACTERISTICS

Patient #	Breed	Age (years)	Gender	Tumor Details	Tumor Location
1	Boxer	10	F	PD: Grade II STS ST: Perivascular wall tumor	Right caudodorsal proximal hind limb
2	Mixed Breed	10	M	PD: Grade II STS ST: Myxosarcoma	Right proximal hind limb
3	Bichon Frise	10	F	PD: Grade III STS	Right caudodorsal proximal hind limb
4	Mixed Breed	7	M	PD: Grade III STS	Left lateral elbow
5	Mixed Breed	12	F	PD: Grade I STS	Left cranio-lateral elbow
6	Miniature Schnauzer	10	M	PD: Grade III STS ST: Myxosarcoma	Left dorsal shoulder
7	Great Dane	10	F	PD: Grade II STS ST: Perivascular wall tumor	Left plantar metatarsus
8	Border Collie	11	M	PD: Malignant mesenchymoma ST: 3 lines of differentiation – osteoblast, fibroblast, lipoblast	Left medial hock
9	Mixed Breed	10	M	PD: Grade I STS ST: Perivascular wall tumor	Right lateral stifle
10	Beagle	12	F	PD: Grade II STS ST: Fibrosarcoma	Left lateral proximal hind limb

PD, primary diagnosis; ST, subtype.

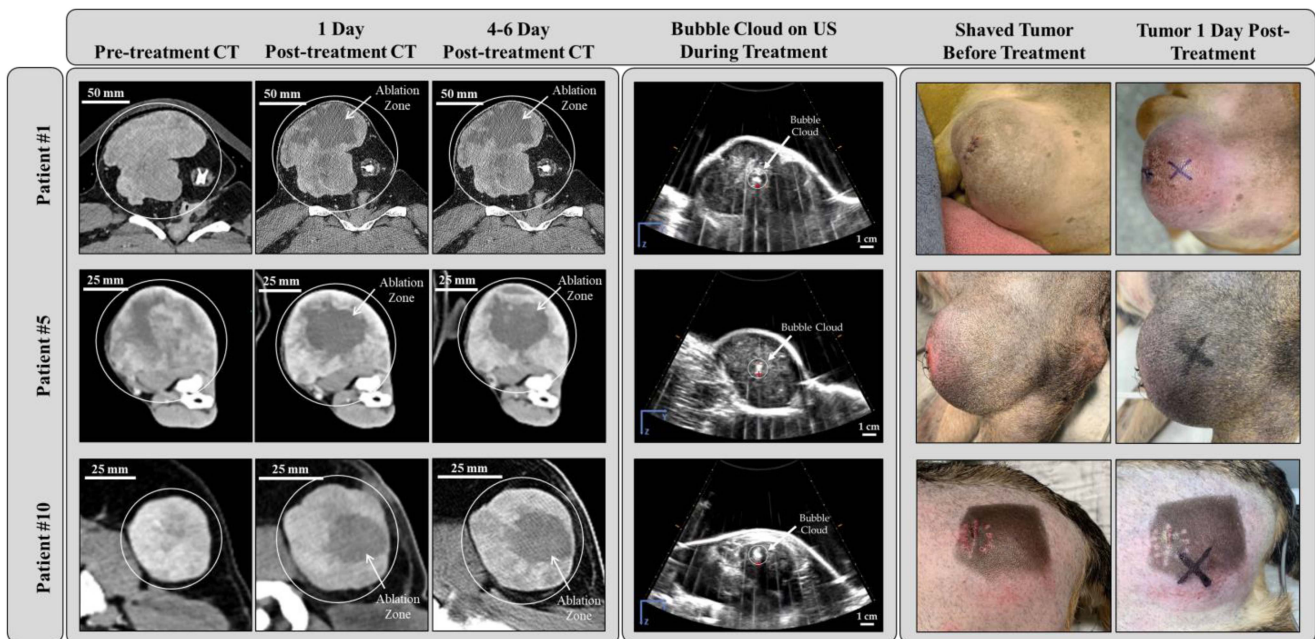


Fig. 3. Histotripsy treatment feasibility and safety were measured using CT and US imaging and adverse event monitoring. Representative images from three canine patients show (from left to right) pre-treatment CT scans of STS (circled), post-treatment CT images with clear regions of histotripsy-ablated tissue 1 day and 4 to 6 days after treatment (arrows), bubble clouds during treatment on real-time US imaging, and various degrees of self-limiting cutaneous injury in the histotripsy treatment path after treatment. Darkened skin on Patient #10 is the result of unrelated sun exposure prior to histotripsy treatment.

examination, or owners' reports. On post-treatment physical examination, swelling was noted for five patients. The masses from nine patients were reported to be warm to the touch post-histotripsy treatment, and erythema of the skin overlying the mass was recorded for five patients. The only histotripsy-related complications noted were various degrees of self-limiting cutaneous injury. Prior to treatment, nine patients had VCOG dermatology AE scores of 1, and one patient had a score of 4.

Following histotripsy treatment, one patient (Patient #1) had an increase in VCOG dermatology AE score from 1 to 2, suspected to be due to pre-focal cavitation damage potential caused in part by hair left behind after shaving at the treatment site in this first patient [Fig. 3]. VCOG dermatology AE scores did not change after histotripsy for the remaining nine patients.

2) Histotripsy Treatment Outcomes: Automated histotripsy ablation treatments were applied to a spherical region

TABLE II
TUMOR AND ABLATION ZONE MEASUREMENTS PRE- AND POST-HISTOTRIPSY

Patient #	Treatment Duration (min)	Tumor Dimensions (cm)			Ablation Zone Dimensions (cm)		
		Pre-treatment	1 Day Post-	4-6 Days Post-	Planned	1 Day Post-	4-6 Days Post-
1	59.5	8.5 x 8.5 x 8.8	9.9 x 8.4 x 10.2	9.2 x 9.3 x 9.9	3 x 3 x 3	5.0 x 4.8 x 4.8	4.7 x 3.9 x 4.0
2	32.1	14.6 x 10.1 x 14.1	16.1 x 10.7 x 15.3	16.7 x 11.4 x 16.2	2.5 x 2.5 x 2.5	Not visible*	Not visible*
3	14.4	5.5 x 4.6 x 4.6	5.3 x 4.5 x 4.6	5.5 x 4.2 x 4.3	2 x 2 x 2	Not visible*	Not visible*
4	33.4	9.2 x 6.5 x 8.4	N/A*	10.3 x 7.0 x 10.1	2.5 x 2.5 x 2.5	N/A**	1.3 x 2.0 x 2.0
5	35.1	6.7 x 4.3 x 6.9	6.7 x 4.2 x 7.0	6.9 x 4.5 x 7.0	2.5 x 2.5 x 2.5	3.2 x 2.7 x 2.7	3.3 x 3.0 x 2.8
6	32.3	16.5 x 6.4 x 9.8	N/A*	17.4 x 7.9 x 10.6	2.5 x 2.5 x 2.5	N/A**	Not visible*
7	33.4	8.4 x 5.4 x 5.5	8.5 x 5.8 x 6.2	8.6 x 6.6 x 6.8	2.5 x 2.5 x 2.5	3.4 x 3.2 x 3.1	1.7 x 2.1 x 1.8
8	15.2	8.1 x 3.9 x 2.3	8.1 x 3.6 x 2.6	8.0 x 3.3 x 2.6	2 x 2 x 2	2.0 x 1.5 x 1.8	1.2 x 0.8 x 1.1
9	15.7	3.7 x 3.4 x 3.1	3.8 x 3.4 x 3.0	3.4 x 3.3 x 3.1	2 x 2 x 2	1.8 x 1.3 x 1.3	1.0 x 0.9 x 0.9
10	33.2	5.3 x 4.1 x 3.8	5.0 x 3.9 x 3.9	5.4 x 4.1 x 4.1	2.5 x 2.5 x 2.5	3.1 x 3.0 x 2.8	2.8 x 2.0 x 2.2

Comparison of pre-, 1 day post-, and 4-6 day post-treatment tumor measurements and ablation zone dimensions as determined by CT imaging. *Ablation zones were not visible on CT scans. **Patients did not receive CT due to scheduling constraints.

within each of the targeted tumors at peak negative pressures (p -) averaging 22.60 ± 7.21 MPa. Depending on the size of the tumor, an ablation volume of either 4.14 cm^3 , 8.18 cm^3 , or 14.14 cm^3 was treated, corresponding to spherical diameters of 2 cm, 2.5 cm, and 3 cm, respectively. When possible, the histotripsy treatment volume was centered in the most solid region of the tumor (determined by pretreatment CT image analysis and physical examinations on the day of treatment). Planned treatment volumes are presented in Table II. Generation of clearly visible histotripsy cavitation bubble clouds on real-time ultrasound imaging was achieved in nine of ten treatments [Fig. 3]. The treatment without bubble cloud visibility was conducted through an intact surgical drape used to couple the patient's amorphous, ulcerated tumor to the degassed water bolus and the histotripsy transducer rather than the open acoustic window used in the other nine patients. To confirm the presence of histotripsy cavitation at the targeted location in this dog, passive cavitation detection was used to measure the backscatter signal of the therapy pulse, similar to approaches used in previous histotripsy studies [37], [41]. In all subjects, cavitation activity was maintained for the duration of the volumetric histotripsy ablation. Treatment times correlated to the volume of the tumor treated, ranging from approximately 14 minutes to 1 hour in length for treatments of 4.19 cm^3 and 14.14 cm^3 in volume, respectively. No significant changes in the echogenicity of the treated regions were noted on ultrasound imaging post-treatment in any of the patients.

3) Computed Tomography Outcomes: Pre-treatment CT images identified clearly demarcated soft tissue tumors of at least 2 cm in diameter for all patients. All tumors had at least two regions of homogenous contrast uptake measuring at least 1 cm in diameter with an accessible treatment window. Comparison of pre- and post-treatment tumor sizes revealed a non-significant increase in tumor size that persisted 4-6 days after histotripsy treatment ($p = 0.191$ 1 day post- vs. pre-; $p = 0.077$ 4-6 day post- vs. pre-) [Table II]. Posttreatment CT images revealed clear, roughly spherical regions of histotripsy ablated tissue in seven of ten patients, visible on CT images

as regions of decreased contrast uptake [Fig. 3]. In the three patients without visible ablation zones on CT, each animal had histologically-evident extensive tumor necrosis in the region of the treated tissue. Measurements of the ablation zone achieved by histotripsy treatment scaled according to planned ablation zone sizes (i.e., larger planned ablation volumes correlated with larger achieved ablation volumes), but measured ablation zones were often greater in size compared to the intended volume. Radiographically measured ablation volumes averaged $10.20 \pm 18.18 \text{ cm}^3$ and $1.60 \pm 10.75 \text{ cm}^3$ larger than planned volumes at 1 day and 4-6 days after treatment, respectively. Although measured volumes were larger than planned volumes when averaged across patients, measured ablation zone volumes were smaller than planned in some patients. Ablation zone volumes were non-significantly reduced 4 days after histotripsy relative to 1 day post histotripsy ($p = 0.063$). Patients 2, 3, and 6 were excluded from analysis because no ablation zone could be definitively measured on CT images; patient 4 because no CT scan was collected 1 day post-histotripsy; and patient 8 because the post-treatment CT scan was taken on day 6. All other patients had 4 day post-histotripsy CT scans with discernable ablation zones.

4) Gross and Histologic Findings: After histotripsy, regions of ablation were clearly identified grossly and histologically in all samples. Grossly, treatment sites were characterized by extensive necrosis and regions of hemorrhage [Fig. 4(a)]. Histologic samples taken from treated regions of the tumors exhibited a mixture of lytic and coagulative cell death and an overall loss of viable tumor cells and cell nuclei, as well as, hemorrhage [Fig. 4(c)]. Clear boundaries were visible between untreated and treated areas of tissue [Fig. 4(d)-(f)].

Complete ablation was observed histologically in all ten dogs within the treated regions of the tumor. Occasionally, small foci of viable tumor cells centered near vessels and infiltrating immune cells, including neutrophils, were observed. No signs of histotripsy-induced damage were observed grossly or microscopically in untreated tissues, and no signs of thermal injury

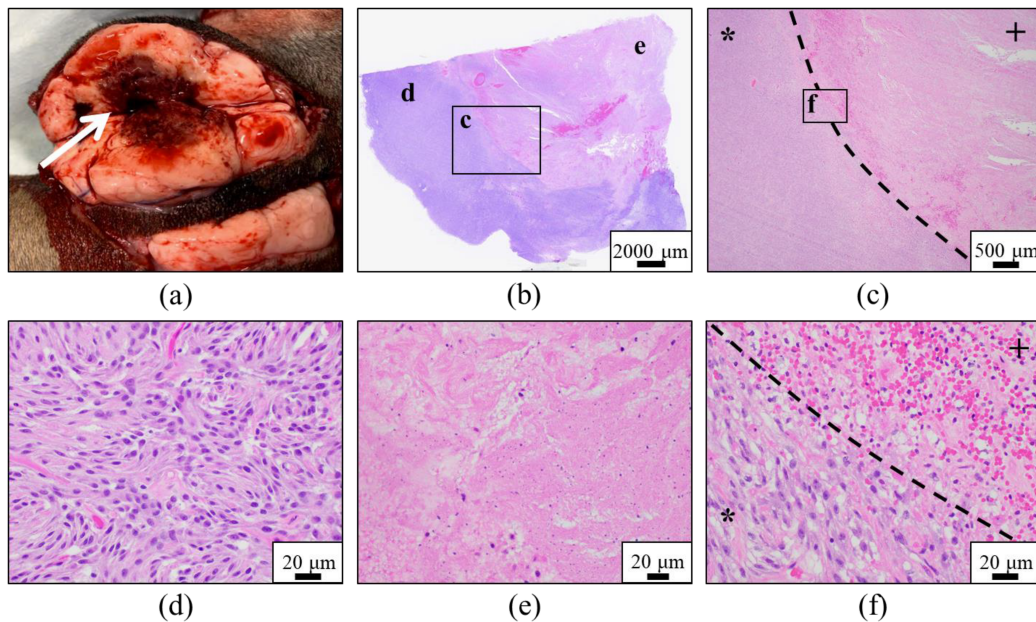


Fig. 4. Representative images demonstrating histotripsy ablation of STS for Patient #5. (a) Gross visualization of lesion characterized by extensive tissue necrosis and hemorrhage (arrow). (b–f) H&E stained sections compared (d) untreated (magnification 40x) and (e) treated (magnification 40x) tumor tissues and (b,c,f) interface regions (c – magnification 2x; f – magnification 40x). Clearly delineated boundaries between treated (+) and untreated (*) tumor tissue were observed.

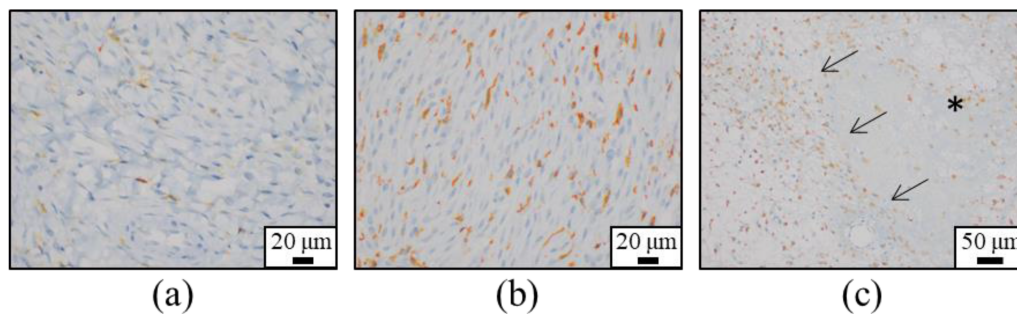


Fig. 5. Multiplex IHC to investigate macrophage populations following histotripsy. Lower numbers of IBA-1/CD206 double positive cells (orange/red) were distributed throughout untreated tumor samples (a) compared to treated samples (b). When captured, the interface between necrotic and intact tumor cells (c) often showed slightly increased numbers of double positive cells (* = area of necrosis; arrows = interface between necrotic and viable cells; a, b – magnification 40x; c – magnification 20x).

were observed within the treatment volumes or overlying tissues in any of the patients.

C. Tumor Microenvironment Following Ablation

1) Multiplex Immunohistochemistry (mIHC) Results: In more than half of all examined samples (7/10), mIHC investigating macrophage populations showed mild to marked increases in IBA-1 and CD206 double-positive cells (red) with macrophage morphology in sections taken from treated tumor [Fig. 5]. Moreover, in untreated tumor samples, these cells were generally loosely distributed throughout intact tumor cells when present, while in treated samples, these often intensified at the interface between necrotic and intact tumor cells. In general, IBA-1/CD206 double positive macrophages were low within necrotic areas. All samples, both treated and untreated, were largely devoid of iNOS positive cells.

Lymphocyte analysis identified aggregates of CD3 positive cells in one tumor, the mesenchymoma, which were readily identifiable in treated samples but not present in untreated samples [Supplementary Fig. 1]. Otherwise, there were generally no significant differences in the lymphocyte staining between treated and untreated sections.

2) Gene Expression Analysis: NanoString differential gene expression analysis identified 79 genes with at least 2-fold upregulation between treated and untreated histotripsy groups [Supplementary Table I, Fig. 6]. One patient (Patient #2) was excluded from statistical analysis because of low housekeeping gene expression. A gene set analysis was performed to group similar pathways. Myeloid compartment, NK cell functions, and interleukin gene sets obtained the highest significance score. Genes associated with inflammation, immune cell migration, and immune cell interactions were the highest upregulated [Supplementary Table II]. Amongst the gene set analyses, the

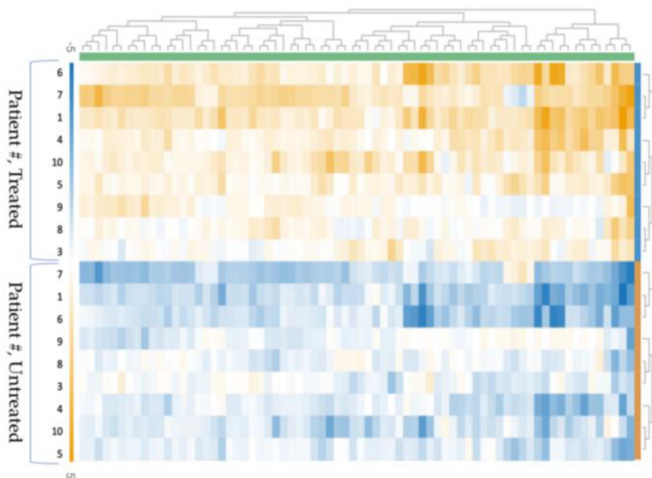


Fig. 6. Hierarchical clustering of 79 differentially expressed immunology genes. Increasing orange intensity indicates increased gene expression and increasing blue intensity indicates decreased gene expression, as shown in the scale bar. According to the differential gene expression profile, samples were clustered with patient held as a confounder and arranged with the treated samples at the top of the figure (blue bar) and the untreated samples at the bottom of the figure (yellow bar).

myeloid compartment gene sets obtained the highest significance score. Further analysis within the myeloid compartment gene sets showed the MARCO gene had the highest fold change. The protein encoded by this gene is a member of the class A scavenger receptor family and is part of the innate antimicrobial immune system. Overall, the gene set analysis indicated an immune-permissive tumor microenvironment.

D. Systemic Immune Response After Histotripsy

1) **Serum Cytokine Analysis:** Serum cytokine concentrations were compared pre-treatment and just prior to surgical resection of the tumor, four to six days post-treatment. There were no statistically-significant changes in the average patient serum cytokine concentrations following histotripsy treatment for any of the analytes. Individual patient serum cytokine concentrations were widely distributed for all analytes both pre- and post-treatment [Supplementary Fig. 2]. Average serum cytokine concentrations ranged from 0.801 pg/mL (IFN γ) to 3.605 pg/mL (IL-8) before histotripsy treatment and 1.088 pg/mL (IL-10) to 3.579 (IL-8) after histotripsy treatment for analytes IL-2, IL-6, IL-7, IL-8, IL-10, IL-15, IL-18, GM-CSF, IFN γ , TNF α , and MCP1 [Supplementary Fig. 3a]. The average serum concentrations for analytes IP-10 and KC-like were higher in value, with values of 23.57 pg/mL and 541.3 pg/L pre-histotripsy and 21.04 pg/mL and 645.7 pg/mL after histotripsy treatment, respectively [Supplementary Fig. 3b,c].

IV. DISCUSSION

This is the first study to demonstrate the safety and feasibility of histotripsy for superficial soft tissue sarcomas (STS). In all patients, histotripsy was successfully generated in the targeted regions, treatments were well-tolerated, and ablation of treated

regions was observed. No significant adverse events associated with histotripsy were reported for any of the patients. Although histotripsy has been previously studied for the ablation of multiple tumor types [8], [9], [10], [12], [13], [14], [15], ablation of superficial tumors, including STS, presents a unique case for histotripsy due to the close proximity of the skin, which has the potential to be damaged by ablative therapies [25], [26], [42]. To minimize this risk, single cycle histotripsy pulses were used for all treatments. Previous studies have shown that single cycle histotripsy, also termed intrinsic threshold histotripsy, appears to be the preferred histotripsy method in cases in which sufficient pressure can be generated and an adequate acoustic window is available, as for STS. Intrinsic threshold histotripsy offers advantages over multi-cycle, shock-scattering histotripsy pulsing regimes by producing a more predictable, dense bubble cloud, allowing a more uniform treatment dose to be applied across the treated tumor volume and minimizing off-target, pre-focal cavitation [37], [43], [44]. In this study, skin injury due to histotripsy was noted only in the first patient that was treated, with all subsequent treatments showing no change in the VCOG-CTCAE score after treatment. The observed skin injury in patient 1 corresponded to extensive pre-focal cavitation visible on real-time ultrasound imaging during treatment. During subsequent treatments, significant pre-focal cavitation was not seen on ultrasound imaging, suggesting that real-time imaging feedback can be used to monitor for these pre-focal cavitation events. Future work should consider optimized methods for preventing and monitoring pre-focal cavitation at the skin.

In all patients, histotripsy bubble clouds were successfully generated within the targeted tumor regions, resulting in precise ablation. The bubble clouds remained visible at the target location throughout the duration of the volumetric treatment and were visualized with real-time ultrasound imaging. After treatment, no significant changes to the echogenicity of the treated tissues were visible on US imaging as has been previously observed for histotripsy [45]. A comparison of pre- and post-treatment CT scans revealed clearly demarcated regions of histotripsy ablation in 7 of the 10 treated patients. In the final three patients, the ablated region could not be clearly visualized despite histologic confirmation of ablation due to necrosis limiting evaluation for lack of contrast uptake. This finding suggests that MRI may be required to more accurately assess post-treatment histotripsy ablation in future studies due to the improved soft tissue contrast that can be achieved without intravenous contrast agent administration, similar to prior histotripsy studies for other applications [46]. MRI is not a routine imaging modality for staging canine patients, but it is the standard imaging modality for human STS patients. In 7 of 10 patients, tumor size measured on CT images increased after histotripsy treatment, possibly due to transient swelling induced by histotripsy ablation. Similarly, post-treatment physical examination identified observable tumor swelling for five patients and tangible warmth of treated masses in nine patients. These findings may be a result of a pro-inflammatory immunogenic response locally in the treated tumor. Radiographically measured ablation volumes were, on average, larger than planned volumes at 1 day and 4-6 days after treatment with no clear

correlation between increased tumor sizes post-treatment and larger than planned ablation volumes. One potential explanation for this finding is that the treatment-induced ablation zone was able to stimulate further cell death in the tissue adjacent to the treatment zone in the 24 hours following histotripsy and before image acquisition. This scenario might also help to explain the aberrant edges to the ablation zone in some CT images. Four days after histotripsy, ablation zones decreased in size relative to one day after histotripsy. Although not statistically significant, this trend is consistent with prior histotripsy studies and suggests the ablation zone had begun to involute and be resorbed by the body. Previous studies characterizing the chronic response to histotripsy ablation in kidney and liver tissues have demonstrated that full resorption of the treated homogenate can take up to 1-2 months [7], [38], making it likely that the ablated STS tissue would have been further resorbed if the tumors had not been surgically removed.

After surgical resection, ablation zones were grossly visible as regions of hemorrhage and necrosis in resected tissues, and histological analysis revealed a near complete removal of viable neoplastic cells in the treated region, with replacement by hemorrhage and acellular debris. In some patients, rare foci of viable tumor cells remained near blood vessels or near the boundaries of the treated lesions, suggesting that the histotripsy dose used in this study should be increased in future studies to ensure complete ablation of the entire targeted tumor volume. The acute immunological effects of histotripsy showed mild to marked increases in alternatively activated macrophages (M2) subjectively observed at the treatment interface. This increase may be due to the normal wound healing response or could possibly represent pro-tumoral tumor-associated macrophages. In the remodeling phase of normal wound healing, M2 macrophages predominate, expressing TGF- β and IL-10 to initiate resolution of inflammation and tissue repair [47]. However, tumor-associated macrophages of the M2 phenotype induced by IL-4 and IL-13 also promote angiogenesis, immune suppression, fibroblast proliferation, and stromal tissue remodeling, which are commonly observed in tumor progression and may promote all steps of the metastatic cascade [48], [49], [50]. The inflammatory phase of wound healing peaks 24-48 hours after injury, with a significant reduction in neutrophils and an increase in macrophages after three days. Macrophage numbers remain high 2-7 days after injury, returning to steady state by day 14 [51]. In our study, post-treatment tumor samples were evaluated 4-6 days following histotripsy; future studies should be conducted to quantify the increases in M2 macrophages and better elucidate their role following histotripsy at various time points after treatment.

Our results from the differential gene expression, routine H&E evaluation, and mIHC consistently reflect a state of inflammation, hemorrhage, and tissue remodeling following histotripsy treatment. The highest differentially-expressed genes, MARCO, SERPINB2, CXCL8, and S100A8/9/12, indicate neutrophil chemotaxis, stress signaling, fibrin and coagulation, and anti-inflammatory (M2) macrophages. These findings are mirrored with the common finding of hemorrhage, hyalinization, and a subjective increase in M2-polarized macrophages. In one tumor sample, aggregates of CD3+ cells were identified

post-treatment. Accumulation of CD3 T lymphocytes is often present in wounds and can be associated with an anti-inflammatory response and granulation tissue formation [52]. However, in the majority of samples, the mIHC lymphocyte panel revealed significant nonspecific staining of CD4 antibody within tumor cells, resulting in high background noise obscuring other chromogen identification and preventing any conclusions regarding lymphocyte tumor infiltration post-treatment to be drawn. Future studies may utilize other methods of immune cell quantification, such as flow cytometry or routine single-stain IHC techniques. Although there were no statistically significant differences between pre- and post-treatment cytokine concentrations for any of the analytes, it is possible that changes were missed due to the timing of cytokine data analysis in this study, which was conducted at various time points prior to histotripsy treatment and surgical removal. Prior studies have observed transient proinflammatory cytokine gene expression after FUS at time points ranging from 6-24 hours post-focused ultrasound [53], [54]. For future studies, having standardized evaluation times obtained more frequently following histotripsy could better illustrate acute systemic immune changes, but can be difficult to achieve using a veterinary patient population due to scheduling constraints with owners.

These results are in line with previous investigations of histotripsy's immunostimulatory potential [9], [12], [15], [16], [18], [19], [20], [21] and suggest that a single histotripsy ablation can alter the local tumor immune microenvironment. Notably, a recent study highlighted that there may be differences in the immune response depending on the percentage of the tumor treated with histotripsy [55]. In this study, histotripsy ablations were applied to either <25% or 50-75% of the total tumor volume in an orthotopic murine model of hepatocellular carcinoma. Decreased immune cell infiltration and delayed homogenate resorption were observed in the <25% group, suggesting that there may be a minimum tumor ablation volume required to generate meaningful immune effects [55]. In the current study, <25% of the total tumor volume was targeted in all ten canine patients. As a result, stronger immune trends may be identified following histotripsy ablation of increased volumes within patient tumors and should be investigated in future studies.

Overall, the results of this study suggest that histotripsy has the potential to be used as a non-invasive therapy for ablation and immunostimulation in patients with STS. However, future work remains to more extensively investigate histotripsy as a potential frontline therapy for STS. While this first treat-and-resect study provides invaluable insight into histotripsy's feasibility, patients still underwent surgery to remove their tumors. Additional studies are warranted to investigate whether histotripsy can ablate complete STS tumors with adequate margins to prevent local recurrence and achieve long-term outcomes equivalent to or superior to surgical resection. Similarly, since STS tumors can grow very large (>5 cm in diameter), and large STS size is a poor predictive factor making surgical resection more difficult [28], future histotripsy studies should explore methods for rapid volumetric ablation of STS tumors, such as previously investigated electronic focal steering methods [56], [57]. Using this approach rather than mechanical steering of the focus through

the treatment volume has previously been shown to significantly reduce treatment times by multiple orders of magnitude. For instance, a previous study by Lundt et al. showed a 40.7 ± 3.1 cm³ volume could be ablated in 42 minutes at a treatment dose of 500 pulses [56]. Another potential approach to ablate large STS tumors is treating the tumor over separate, repeated sessions, similar to approaches used for fractionated radiation therapy treatments [58]. In addition to reducing the time per treatment session and lowering risks associated with prolonged anesthesia, applying repeated treatments might offer an added advantage of re-stimulating an already primed immune response to elicit additional systemic benefits. Repeated, partial treatments of the primary tumor might also avoid complications caused by ablation-related cytokine storms and/or immune cell hyperactivation, which could result from large volume ablations and have been observed for other ablation methods [59], [60]. These potential methods for treating STS with histotripsy in single and multiple sessions should be investigated in future trials, along with more extensive characterization of the chronic immune responses after partial and complete STS tumor ablation.

V. CONCLUSION

The results of this study demonstrate histotripsy's potential as a precise, non-invasive treatment for soft tissue sarcoma. This treat-and-resect study showed histotripsy was well-tolerated and effective in canine patients with spontaneous STS. Early immunological results suggest that histotripsy was able to induce pro-immunogenic changes in the local tumor microenvironment. Future trials investigating histotripsy for complete tumor ablation and characterizing the chronic response after histotripsy treatment are warranted.

ACKNOWLEDGMENT

The authors would like to thank Dr. Kelsie Timbie and the FUS Foundation for their support of this work. We would also like to thank the following team members for their contributions to this trial: Clinical Research Office – Mindy Quigley and Courtney Snead; Veterinarians involved in patient care – Brittany Ciepluch, Keiko Murakami, Jennifer Carroll, and Katherine Kierski; Licensed Veterinary Technicians – Stefanie Olsen and Maryann Cline; Clinical Business Office fund management – Christy Barry; and the Teaching and Research Animal Care Support Services at Virginia Tech. This study was facilitated by the Translational Science Shared Resource, Hollings Cancer Center, Medical University of South Carolina (P30 CA138313) and the National Institutes of Health (R01CA269811).

REFERENCES

- [1] M. Hoogenboom et al., "Mechanical high-intensity focused ultrasound destruction of soft tissue: Working mechanisms and physiologic effects," *Ultrasound Med. Biol.*, vol. 41, no. 6, pp. 1500–1517, 2015, doi: [10.1016/j.ultrasmedbio.2015.02.006](https://doi.org/10.1016/j.ultrasmedbio.2015.02.006).
- [2] K. Bader et al., "For whom the bubble grows: Physical principles of bubble nucleation and dynamics in histotripsy ultrasound therapy," *Ultrasound Med. Biol.*, vol. 45, no. 5, pp. 1056–1080, 2019, doi: [10.1016/j.ultrasmedbio.2018.10.035](https://doi.org/10.1016/j.ultrasmedbio.2018.10.035).
- [3] E. Vlasisavljevic et al., "Visualizing the histotripsy process: Bubble cloud-cancer cell interactions in a tissue-mimicking environment," *Ultrasound Med. Biol.*, vol. 42, no. 10, pp. 2466–2477, 2016, doi: [10.1016/j.ultrasmedbio.2016.05.018](https://doi.org/10.1016/j.ultrasmedbio.2016.05.018).
- [4] Z. Xu et al., "Histotripsy: The first noninvasive, non-ionizing, non-thermal ablation technique based on ultrasound," *Int. J. Hyperthermia*, vol. 38, no. 1, pp. 561–575, 2021, doi: [10.1080/02656736.2021.1905189](https://doi.org/10.1080/02656736.2021.1905189).
- [5] E. Vlasisavljevic et al., "Histotripsy-induced cavitation cloud initiation thresholds in tissues of different mechanical properties," *IEEE Trans. Ultrasonics, Ferroelect., Freq. Control*, vol. 61, no. 2, pp. 341–352, Feb. 2014, doi: [10.1109/TUFFC.2014.6722618](https://doi.org/10.1109/TUFFC.2014.6722618).
- [6] E. Vlasisavljevic et al., "Effects of tissue stiffness, ultrasound frequency, and pressure on histotripsy-induced cavitation bubble behavior," *Phys. Med. Biol.*, vol. 60, no. 6, pp. 2271–2292, 2015, doi: [10.1088/0031-9155/60/6/2271](https://doi.org/10.1088/0031-9155/60/6/2271).
- [7] T. Hall et al., "Histotripsy of rabbit renal tissue in vivo: Temporal histologic trends," *J. Endourol.*, vol. 21, no. 10, pp. 1159–1166, 2007, doi: [10.1089/end.2007.9915](https://doi.org/10.1089/end.2007.9915).
- [8] G. Schade et al., "Histotripsy focal ablation of implanted prostate tumor in an ACE-I canine cancer model," *J. Urol.*, vol. 188, no. 5, pp. 1957–1964, 2012, doi: [10.1016/j.juro.2012.07.006](https://doi.org/10.1016/j.juro.2012.07.006).
- [9] G. Schade et al., "Boiling histotripsy ablation of renal cell carcinoma in the eker rat promotes a systemic inflammatory response," *Ultrasound Med. Biol.*, vol. 45, no. 1, pp. 137–147, 2019, doi: [10.1016/j.ultrasmedbio.2018.09.006](https://doi.org/10.1016/j.ultrasmedbio.2018.09.006).
- [10] L. Arnold et al., "Histotripsy ablation of bone tumors: Feasibility study in excised canine osteosarcoma tumors," *Ultrasound Med. Biol.*, vol. 47, no. 12, pp. 3435–3446, 2021, doi: [10.1016/j.ultrasmedbio.2021.08.004](https://doi.org/10.1016/j.ultrasmedbio.2021.08.004).
- [11] T. Gerhardson et al., "Histotripsy mediated immunomodulation in a mouse GL261 intracranial glioma model," in *Proc. Int. Symp. Therapeutic Ultrasound*, 2018, Art. no. 51845, doi: [10.13140/RG.2.2.19788.51845](https://doi.org/10.13140/RG.2.2.19788.51845).
- [12] A. Hendricks-Wenger et al., "Histotripsy ablation alters the tumor microenvironment and promotes immune system activation in a subcutaneous model of pancreatic cancer," *IEEE Trans. Ultrasonics, Ferroelect., Freq. Control*, vol. 68, no. 9, pp. 2987–3000, Sep. 2021, doi: [10.1109/TUFFC.2021.3078094](https://doi.org/10.1109/TUFFC.2021.3078094).
- [13] T. Worlikar et al., "Histotripsy for non-invasive ablation of hepatocellular carcinoma (HCC) tumor in a subcutaneous xenograft murine model," in *Proc. 40th Annu. Int. Conf. IEEE Eng. Med. Biol. Soc.*, 2018, pp. 6064–6067, doi: [10.1109/EMBC.2018.8513650](https://doi.org/10.1109/EMBC.2018.8513650).
- [14] A. Hendricks-Wenger et al., "Histotripsy for the treatment of cholangiocarcinoma liver tumors: In vivo feasibility and ex vivo dosimetry study," *IEEE Trans. Ultrasonics, Ferroelect., Freq. Control*, vol. 68, no. 9, pp. 2953–2964, Sep. 2021, doi: [10.1109/TUFFC.2021.3073563](https://doi.org/10.1109/TUFFC.2021.3073563).
- [15] J. J. Vidal et al., "Phase I study of safety and efficacy of hepatic histotripsy: Preliminary results of first in man experience with robotically-assisted sonic therapy," *Int. Soc. Therapeutic Ultrasound*, vol. 42, no. 7, pp. 1016–1023, 2019.
- [16] A. Hendricks-Wenger et al., "Immunological effects of histotripsy for cancer therapy," *Front. Oncol., Rev.*, vol. 11, 2021, Art. no. 681629, doi: [10.3389/fonc.2021.681629](https://doi.org/10.3389/fonc.2021.681629).
- [17] R. J. van den Bijgaart et al., "Thermal and mechanical high-intensity focused ultrasound: Perspectives on tumor ablation, immune effects and combination strategies," *Cancer Immunol., Immunotherapy*, vol. 66, no. 2, pp. 247–258, 2017, doi: [10.1007/s00262-016-1891-9](https://doi.org/10.1007/s00262-016-1891-9).
- [18] Y. J. Ho et al., "Ultrasound in tumor immunotherapy: Current status and future developments," *J. Controlled Release*, vol. 323, pp. 12–23, 2020, doi: [10.1016/j.jconrel.2020.04.023](https://doi.org/10.1016/j.jconrel.2020.04.023).
- [19] S. Qu et al., "Non-thermal histotripsy tumor ablation promotes abscopal immune responses that enhance cancer immunotherapy," *J. for Immunotherapy Cancer*, vol. 8, no. 1, 2020, Art. no. e000200, doi: [10.1136/jitc-2019-000200](https://doi.org/10.1136/jitc-2019-000200).
- [20] K. Pakh et al., "Boiling Histotripsy-induced partial mechanical ablation modulates tumour microenvironment by promoting immunogenic cell death of cancers," *Sci. Rep.*, vol. 9, 2019, Art. no. 9050, doi: [10.1038/s41598-019-45542-z](https://doi.org/10.1038/s41598-019-45542-z).
- [21] J. J. Vidal et al., "Liver histotripsy mediated abscopal effect—Case report," *IEEE Trans. Ultrasonics, Ferroelect., Freq. Control*, vol. 68, no. 9, pp. 3001–3005, Sep. 2021, doi: [10.1109/TUFFC.2021.3100267](https://doi.org/10.1109/TUFFC.2021.3100267).
- [22] A. Antoniou et al., "Treatment of canine and feline sarcoma using MR-guided focused ultrasound system," *J. Ultrasound*, pp. 1–10, 2022. [Online]. Available: <https://link.springer.com/article/10.1007/s40477-022-00672-5>
- [23] M. C. Seward et al., "Feasibility of targeting canine soft tissue sarcoma with MR-guided high-intensity focused ultrasound," *Int. J. Hyperthermia*, vol. 35, no. 1, pp. 205–215, 2019, doi: [10.1080/02656736.2018.1489072](https://doi.org/10.1080/02656736.2018.1489072).

- [24] J. Carroll et al., "High intensity focused ultrasound for the treatment of solid tumors: A pilot study in canine cancer patients," *Int. J. Hyperthermia*, vol. 39, no. 1, pp. 855–864, 2022, doi: [10.1080/02656736.2022.2097323](https://doi.org/10.1080/02656736.2022.2097323).
- [25] F. Wu et al., "Extracorporeal focused ultrasound surgery for treatment of human solid carcinomas: Early Chinese clinical experience," *Ultrasound Med. Biol.*, vol. 30, no. 2, pp. 245–260, 2004, doi: [10.1016/j.ultrasmedbio.2003.10.010](https://doi.org/10.1016/j.ultrasmedbio.2003.10.010).
- [26] W. Yu et al., "Significance of HIFU in local unresectable recurrence of soft tissue sarcoma, a single-center, retrospective, case series in China," *Surg. Oncol.*, vol. 30, pp. 117–121, 2019, doi: [10.1016/j.suronc.2019.06.004](https://doi.org/10.1016/j.suronc.2019.06.004).
- [27] J. Shim et al., "Pediatric sarcomas are targetable by MR-Guided high intensity focused ultrasound (MR-HIFU): Anatomical distribution and radiological characteristics," *Pediatr. Blood Cancer*, vol. 63, no. 10, pp. 1753–1760, 2016, doi: [10.1002/psc.26079](https://doi.org/10.1002/psc.26079).
- [28] M. M. Dennis et al., "Prognostic factors for cutaneous and subcutaneous soft tissue sarcomas in dogs," *Vet. Pathol.*, vol. 48, no. 1, pp. 73–84, 2011, doi: [10.1177/0300985810388820](https://doi.org/10.1177/0300985810388820).
- [29] A. C. Gamboa et al., "Soft-tissue sarcoma in adults: An update on the current state of histiotypic-specific management in an era of personalized medicine," *CA Cancer J. Clin.*, vol. 70, no. 3, pp. 200–229, 2020, doi: [10.3322/caac.21605](https://doi.org/10.3322/caac.21605).
- [30] J. D. Schiffman and M. Breen, "Comparative oncology: What dogs and other species can teach us about humans with cancer," *Philos. Trans. Roy. Soc. Lond B Biol. Sci.*, vol. 370, no. 1673, 2015, Art. no. 20140231, doi: [10.1098/rstb.2014.0231](https://doi.org/10.1098/rstb.2014.0231).
- [31] A. K. LeBlanc and C. N. Mazcko, "Improving human cancer therapy through the evaluation of pet dogs," *Nature Rev. Cancer*, vol. 20, no. 12, pp. 727–742, 2020, doi: [10.1038/s41568-020-0297-3](https://doi.org/10.1038/s41568-020-0297-3).
- [32] M. I. Carvalho et al., "The dog as a model to study the tumor microenvironment," *Adv. Exp. Med. Biol.*, vol. 1329, pp. 123–152, 2021, doi: [10.1007/978-3-030-73119-9_7](https://doi.org/10.1007/978-3-030-73119-9_7).
- [33] C. E. McCarthy et al., "Developing and validating model systems for immuno-oncology," *Cancer Cell*, vol. 39, no. 8, pp. 1018–1022, 2021, doi: [10.1016/j.ccell.2021.05.017](https://doi.org/10.1016/j.ccell.2021.05.017).
- [34] S. K. Von Rueden and T. M. Fan, "Cancer-Immunity cycle and therapeutic Interventions- Opportunities for including pet dogs with cancer," *Front. Oncol.*, vol. 11, 2021, Art. no. 773420, doi: [10.3389/fonc.2021.773420](https://doi.org/10.3389/fonc.2021.773420).
- [35] J. Parsons et al., "Cost-effective assembly of a basic fiber-optic hydrophone for measurement of high-amplitude therapeutic ultrasound fields," *J. Acoust. Soc. Amer.*, vol. 119, no. 3, pp. 1432–1440, 2006, doi: [10.1121/1.2166708](https://doi.org/10.1121/1.2166708).
- [36] J. E. Parsons et al., "Pulsed cavitation ultrasound therapy for controlled tissue homogenization," *Ultrasound Med. Biol.*, vol. 32, no. 1, pp. 115–129, 2006, doi: [10.1016/j.ultrasmedbio.2005.09.005](https://doi.org/10.1016/j.ultrasmedbio.2005.09.005).
- [37] E. Vlasisavljevič et al., "Effects of ultrasound frequency and tissue stiffness on the histotripsy intrinsic threshold for cavitation," *Ultrasound Med. Biol.*, vol. 41, no. 6, pp. 1651–67, 2015, doi: [10.1016/j.ultrasmedbio.2015.01.028](https://doi.org/10.1016/j.ultrasmedbio.2015.01.028).
- [38] E. Vlasisavljevič et al., "Non-Invasive ultrasound liver ablation using histotripsy: Chronic study in an in vivo rodent model," *Ultrasound Med. Biol.*, vol. 42, no. 8, pp. 1890–1902, 2016, doi: [10.1016/j.ultrasmedbio.2016.03.018](https://doi.org/10.1016/j.ultrasmedbio.2016.03.018).
- [39] E. Vlasisavljevič et al., "Image-Guided non-invasive ultrasound liver ablation using histotripsy: Feasibility study in an in vivo porcine model," *Ultrasound Med. Biol.*, vol. 39, no. 8, pp. 1398–1409, 2013, doi: [10.1016/j.ultrasmedbio.2013.02.005](https://doi.org/10.1016/j.ultrasmedbio.2013.02.005).
- [40] A. K. LeBlanc et al., "Veterinary cooperative oncology group-common terminology criteria for adverse events (VCOG-CTCAE v2) following investigational therapy in dogs and cats," *Vet. Comp. Oncol.*, vol. 19, no. 2, pp. 311–352, 2021, doi: [10.1111/vco.12677](https://doi.org/10.1111/vco.12677).
- [41] X. Zhang et al., "Non-invasive thrombolysis using microtripsy: A parameter study," *IEEE Trans. Ultrasonics, Ferroelect. Control*, vol. 62, no. 12, pp. 2092–2105, Dec. 2015, doi: [10.1109/TUFFC.2015.007268](https://doi.org/10.1109/TUFFC.2015.007268).
- [42] J.-J. Li et al., "Complications of high intensity focused ultrasound for patients with hepatocellular carcinoma," *Technol. Cancer Res. Treat.*, vol. 8, no. 3, pp. 217–224, 2009, doi: [10.1177/153303460900800306](https://doi.org/10.1177/153303460900800306).
- [43] K.-W. Lin et al., "Histotripsy beyond the intrinsic cavitation threshold using very short ultrasound pulses: Microtripsy," *IEEE Trans. Ultrasonics, Ferroelect. Control*, vol. 61, no. 2, pp. 251–265, Feb. 2014, doi: [10.1109/TUFFC.2014.6722611](https://doi.org/10.1109/TUFFC.2014.6722611).
- [44] A. Maxwell et al., "Cavitation clouds created by shock scattering from bubbles during histotripsy," *J. Acoust. Soc. Amer.*, vol. 130, no. 4, pp. 1888–1898, 2011, doi: [10.1121/1.3625239](https://doi.org/10.1121/1.3625239).
- [45] T. L. Hall and J. B. Fowlkes, "A real-time measure of cavitation induced tissue disruption by ultrasound imaging backscatter reduction," *IEEE Trans. Ultrasonics, Ferroelect. Control*, vol. 54, no. 3, pp. 569–575, Mar. 2007, doi: [10.1109/TUFFC.2007.279](https://doi.org/10.1109/TUFFC.2007.279).
- [46] A. R. Smolock et al., "Robotically assisted sonic therapy as a noninvasive nonthermal ablation modality: Proof of concept in a porcine liver model," *Radiology*, vol. 287, no. 2, pp. 485–493, 2018, doi: [10.1148/radiol.2018171544](https://doi.org/10.1148/radiol.2018171544).
- [47] Y. Hua and G. Bergers, "Tumors vs. Chronic wounds: An immune cell's perspective," *Front. Immunol.*, vol. 10, 2019, Art. no. 2178, doi: [10.3389/fimmu.2019.02178](https://doi.org/10.3389/fimmu.2019.02178).
- [48] J. Liu et al., "New insights into M1/M2 macrophages: Key modulators in cancer progression," *Cancer Cell Int.*, vol. 21, no. 1, 2021, Art. no. 389, doi: [10.1186/s12935-021-02089-2](https://doi.org/10.1186/s12935-021-02089-2).
- [49] Y. Deng et al., "Sphingomyelin synthase 2 facilitates M2-like macrophage polarization and tumor progression in a mouse model of triple-negative breast cancer," *Acta Pharm. Sinica*, vol. 42, no. 1, pp. 149–159, 2021, doi: [10.1038/s41401-020-0419-1](https://doi.org/10.1038/s41401-020-0419-1).
- [50] Y. Lin et al., "Tumor-associated macrophages in tumor metastasis: Biological roles and clinical therapeutic applications," *J. Hematol. Oncol.*, vol. 12, no. 1, 2019, Art. no. 76, doi: [10.1186/s13045-019-0760-3](https://doi.org/10.1186/s13045-019-0760-3).
- [51] S. Aitchison et al., "Skin wound healing: Normal macrophage function and macrophage dysfunction in diabetic wounds," *Molecules*, vol. 26, no. 16, 2021, Art. no. 4917, doi: [10.3390/molecules26164917](https://doi.org/10.3390/molecules26164917).
- [52] X. Wang et al., "T lymphocytes attenuate dermal scarring by regulating inflammation, neovascularization, and extracellular matrix remodeling," *Adv. Wound Care*, vol. 8, no. 11, pp. 527–537, 2019, doi: [10.1089/wound.2019.0981](https://doi.org/10.1089/wound.2019.0981).
- [53] D. McMahon et al., "Acute effects of focused ultrasound-induced increases in blood-brain barrier permeability on rat microvascular transcriptome," *Sci. Rep.*, vol. 7, 2017, Art. no. 45657, doi: [10.1038/srep45657](https://doi.org/10.1038/srep45657).
- [54] Z. I. Kovacs et al., "Disrupting the blood-brain barrier by focused ultrasound induces sterile inflammation," *Proc. Nat. Acad. Sci. United States Amer.*, vol. 114, no. 1, pp. E75–E84, 2017, doi: [10.1073/pnas.1614777114](https://doi.org/10.1073/pnas.1614777114).
- [55] T. Worlikar et al., "Impact of histotripsy on development of intrahepatic metastases in a rodent liver tumor model," *Cancers*, vol. 14, no. 7, 2022, Art. no. 1612, doi: [10.3390/cancers14071612](https://doi.org/10.3390/cancers14071612).
- [56] J. Lundt et al., "Noninvasive, rapid ablation of tissue volume using histotripsy," *Ultrasound Med. Biol.*, vol. 43, no. 12, pp. 2834–2847, 2017, doi: [10.1016/j.ultrasmedbio.2017.08.006](https://doi.org/10.1016/j.ultrasmedbio.2017.08.006).
- [57] T. Gerhardson et al., "Effect of frequency and focal spacing on transcranial histotripsy clot liquefaction, using electronic focal steering," *Ultrasound Med. Biol.*, vol. 43, no. 10, pp. 2302–2317, 2017, doi: [10.1016/j.ultrasmedbio.2017.06.010](https://doi.org/10.1016/j.ultrasmedbio.2017.06.010).
- [58] R. L. M. Haas et al., "Preoperative radiotherapy for extremity soft tissue sarcoma; past, present and future perspectives on dose fractionation regimens and combined modality strategies," *Radiotherapy Oncol.*, vol. 119, no. 1, pp. 14–21, 2016, doi: [10.1016/j.radonc.2015.12.002](https://doi.org/10.1016/j.radonc.2015.12.002).
- [59] J. K. Seifert and D. L. Morris, "World survey on the complications of hepatic and prostate cryotherapy," *World J. Surg.*, vol. 23, no. 2, pp. 109–114, 1999, doi: [10.1007/pl00013173](https://doi.org/10.1007/pl00013173).
- [60] T. M. Wah et al., "Image-guided percutaneous radiofrequency ablation and incidence of post-radiofrequency ablation syndrome: Prospective survey," *Radiology*, vol. 237, no. 3, pp. 1097–1102, 2005, doi: [10.1148/radiol.2373042008](https://doi.org/10.1148/radiol.2373042008).